Available online at www.sciencedirect.com
SCIENCE DIRECT
Journal of Power Sources 157 (2006) 515–521
JOURNAL OF POWER SOURCES
www.elsevier.com/locate/jpowsour

# Rotating ring–disk electrode measurements on Mn dissolution and capacity losses of spinel electrodes in various organic electrolytes

Jenn-Shing Chen [a,*], Li-Fang Wang [b,**], Bor-Jian Fang [b], Shao-Yung Lee [c], Ren-Zheng Guo [c]

[a] *Department of Applied Chemistry, National University of Kaohsiung, Kaohsiung City, Taiwan 811, ROC*
[b] *College of Life Science, Kaohsiung Medical University, Kaohsiung City, Taiwan 807, ROC*
[c] *Department of Chemical Engineering, I-Shou University, Kaohsiung County, Taiwan 840, ROC*

Received 29 June 2005; accepted 18 August 2005
Available online 24 October 2005

**Abstract**

The Mn dissolution and capacity losses of spinel electrodes in lithium-ion cells with the various electrolyte solutions of $LiPF_6$, $LiClO_4$, $LiBF_4$ and $LiCF_3SO_3$, in ethylene carbonate–dimethyl carbonate (EC–DMC) were studied using rotating ring–disk collection experiments. The cyclic voltammograms are similar at high scan rates for all electrolytes. Electrodes with $LiPF_6$ electrolyte show the best cycling performance. Cells with both $LiPF_6$ and $LiBF_4$ electrolyte solutions exhibited a capacity loss of 0.45% per cycle over 200 cycles at high scan rates, and these were slightly lower than the 0.5% per cycle in $LiClO_4$ and $LiCF_3SO_3$ electrolytes. The in situ monitoring of Mn dissolution from various electrolytes was carried out under different conditions. Ring cathodic currents of similar shaped were obtained for all electrolytes, which reveal that the Mn dissolution from the spinel $LiMn_2O_4$ electrodes exists and the highest Mn dissolution takes place at the top of charge voltage in all of electrolytes. Under both overcharge and overdischarge conditions, the ring current peak at disk potential of 5.0 V in the $LiCF_3SO_3$ electrolyte is much larger than that in other electrolytes. Moreover, the increase in ring current with cycle number occurs only in the $LiCF_3SO_3$ electrolyte. These results can be attributed to the oxidation of $LiCF_3SO_3$ electrolyte due to its voltage breakdown below 5.0 V.


*Keywords:* Lithium-ion cell; Spinel cathode ($LiMn_2O_4$); Electrolyte; Rotating ring–disk electrode

## 1. Introduction

In the past decade, $LiMn_2O_4$ type of spinel materials has been studied extensively for lithium-ion (Li-ion) batteries as a cathode material because of its high voltage, low cost, safer performance and environmental benign nature. These attractive characteristics make spinel $LiMn_2O_4$ a good candidate for use in large-scale Li-ion batteries for electric vehicle (EV) and hybrid electric vehicle (HEV) applications [1]. Nevertheless, capacity fading during charge–discharge cycling is a problem for the spinel, particularly at elevated temperatures. Several factors have been proposed to contribute to capacity fading such as spinel dissolution [2–9], the Jhan–Teller effect [5,10,11] and/or lattice instability [12–15]. Of these factors, most of the evidences reported so far points to manganese dissolution at the top of charge as the major reason for capacity fading. Thus, it is essential to investigate the dissolution behavior of the spinel electrode in order to reduce the level of capacity fading. We have recently used rotating ring–disk collection experiments to measure the Mn dissolution from a thin porous spinel $LiMn_2O_4$ electrode [16,17]. The in situ monitoring of Mn dissolution from the different types of spinel $LiMn_2O_4$ electrodes was examined in terms of cycle number, temperature, overcharge and overdischarge. The findings provided a clear understanding of the Mn dissolution behavior of the different types of $LiMn_2O_4$ spinels and the variation in manganese concentration in the electrolyte during cycling.

Liquid non-aqueous $Li^+$-conducting organic electrolytes are mostly used in commercial lithium secondary batteries of today. Many papers have reported that the Mn dissolution is a strong function of the nature of lithium salts added [18–23]. It has been shown that Mn dissolution was induced by acids generated by reaction of fluorinated anions with water impurities present in the cell components (electrode, electrolytes), oxidation of the

* Corresponding author. Tel.: +886 7 591 9463; fax: +886 7 591 9348.
** Corresponding author. Tel.: +886 7 312 1101; fax: +886 7 312 5339.
*E-mail addresses:* jschen@nuk.edu.tw (J.-S. Chen), lfwang@kmu.edu.tw (L.-F. Wang).

0378-7753/$ – see front matter © 2005 Elsevier B.V. All rights reserved.
doi:10.1016/j.jpowsour.2005.08.019

solvent and instability of Li-based salt [4,20–25]. In order to minimize the solubility of the spinel electrode, one of strategies suggested is to use an electrolyte with salts other than $LiPF_6$ and eliminate water contamination [19,26]. Although various liquid organic electrolytes have been tested for lithium secondary cells as electrolyte solutions, the results are still not very satisfactory [18,19]. In the present study, we investigated the Mn dissolution behavior in various electrolyte solutions comprising different lithium salts using the rotating ring–disk electrode (RRDE) technique. The organic electrolyte solutions used were mixtures of EC and DMC (1:1, v/v) and 1 M lithium salts such as $LiPF_6$, $LiClO_4$, $LiBF_4$ and $LiCF_3SO_3$. The effect of various electrolyte salts on Mn dissolution and capacity losses in lithium-ion cells were studied.

## 2. Experimental

Composite disk cathodes were prepared by wet coating, and were made from stoichometric spinel $LiMn_2O_4$ (EM Merck), acetylene black, SFG-6 (Timcal) and polyvinylidene fluoride (PVDF) binder (MKB-212C, Elf Atochem) in a weight ratio of 86:2:4:6. Spinel $LiMn_2O_4$, acetylene black and SFG-6 were first added to a solution of PVDF in *n*-methyl-2-pyrrolidone (NMP, Riedel-deHaen). The mixture was stirred for 20 min at room temperature with a magnetic bar, and then with a turbine for 5 min at 2000 rpm to form a slurry having the appropriate viscosity. The resulting slurry was coated onto a stainless-steel disk (diameter: 6 mm) and dried at 120 °C for 40 min. The resulting coating had a thickness of ∼100 μm and an active material mass of ∼2.4 mg. The quantity of active materials on the disk electrodes was kept constant (±0.2 mg). The disk electrodes were dried overnight at 100 °C under vacuum before being transferred to an argon-filled glove box for cell assembly.

The RRDE system (AFMT134DCPTT, Pine Instruments) with interchangeable discs consisted of a 6 mm diameter stainless steel disk electrode and a Pt ring electrode (width: 1 mm) that were separated with a 0.5 mm gap. The collection efficiency when using this geometry was 0.24. The rotating ring–disk assembly was operated by means of a Pine AFMSRX rotator and CH705 Bipotentiostat (CH Instruments) with a computerized interface. The manganese dissolved from the disk electrode was collected at the Pt ring. Lithium foil (Aldrich) was used for both the reference and counter electrodes. A schematic of a glass-beaker cell containing the RRDE system was given in our earlier paper [16]. Various Li-based salts (1.0M) including lithium hexafluorophosphate ($LiPF_6$), lithium perchlorate ($LiClO_4$), lithium tetrafluoroborate ($LiBF_4$) and lithium trifluoromethanesulfate ($LiCF_3SO_3$) in a 1:1 (v/v) mixture of ethylene carbonate (EC) and dimethyl carbonate (DMC) were used as the different electrolytes (Ferro Corp.). A glass-beaker cell, filled with 10 ml electrolyte, was used for electrochemical cycling and the $Mn^{2+}$ ion collection experiments. During cyclic voltammograms, the potential of the spinel $LiMn_2O_4$ disk electrode was scanned between 3.0 and 4.5 V versus $Li/Li^+$ at 10 mV $s^{-1}$. The Li anode was isolated from the cathode by two layers of Celgard 3401 separator and the Li reference electrode by a vycor tip to avoid dissolved Mn ions being deposited on the Li anode and reference electrode. For the in situ cell test, the spinel $LiMn_2O_4$ disk was cycled at 100 mV $s^{-1}$ between a 3.0 and 4.5 V or extended voltage range at various conditions while the ring was held at 1.0 V to collect the $Mn^{2+}$ ions generated from the disk electrode. Three tests were carried out for each condition and the average performance was recorded. The cell fabrication and all measurements were carried out in a glove box filled with dry argon.

## 3. Results and discussion

The Mn dissolution and capacity losses of spinel electrodes in lithium-ion cells are critically dependent on the nature of lithium salts added. In order to understand the effect of lithium salt on Mn dissolution, the performance of four groups, A, B, C and D, which represent the spinel $LiMn_2O_4$ cathode powders in 1.0 M-$LiPF_6$–EC/DMC, 1.0 M-$LiClO_4$–EC/DMC, 1.0 M-$LiBF_4$–EC/DMC and 1.0 M-$LiCF_3SO_3$–EC/DMC electrolytes, respectively, was investigated. Cyclic voltammograms (CVs) were obtained at room temperature (∼30 °C) between 4.5 and 3.0 V versus $Li/Li^+$ at 10 mV $s^{-1}$ and 500 rpm. The resulting data for samples A, B, C and D at 1, 50, 100, 150 and 200 cycles are shown in Fig. 1. The shapes of these four curves are similar at a very high scan rate (10 mV $s^{-1}$), although the height of the peak decreases during consecutive cycling. Generally, the typical CV of the spinel electrode exhibits two peaks located at 4.03 and 4.17 V on charge and at 3.99 and 4.10 V on discharge. These two peaks correspond to the two-step reversible (de)intercalation of lithium between $LiMn_2O_4$ and λ-MnO. However, for the higher scan rate, the reaction zone is limited to a small thickness on the surface of the electrode and the two peaks are not well separated. As seen from Fig. 1, the disk current is only observed after 4 V on the anodic scan (during charge) and decreases continuously until 3.3 V on the cathodic scan (during discharge). Both the anodic and cathodic peak currents for the four samples decreased significantly during the first 50 cycles. This suggests that the spinel disk electrodes, which initially lose capacity rapidly with cycling in all different electrolytes, begin to exhibit capacity retention after about 50 cycles. Fig. 2 shows a plot of high-rate discharge capacity versus cycle number for the four samples. The discharge capacity is calculated from the CVs in Fig. 1. The discharge capacity declined to less than 10 mAh $g^{-1}$ for all of samples by the end of 200 high-rate cycles. As has been commonly reported in the literature [18,19], the $LiPF_6$-salt electrolyte (sample A) shows clearly the best cycling performance and the $LiCF_3SO_3$–salt electrolyte (sample D) has the lowest discharge capacity. $LiPF_6$ has the best cycling performance owing to its higher oxidation potential and specific conductivity. For these four kinds of solute EC/DMC electrolytes, the order of increasing oxidation potential is $LiPF_6 > LiBF_4 > LiClO_4 > LiCF_3SO_3$ and the order of increasing specific conductivity is $LiPF_6 > LiClO_4 > LiBF_4 > LiCF_3SO_3$ [18,21]. Moreover, the specific discharge capacity obtained for the first cycle varies from 25.6 mAh $g^{-1}$ (sample A) to 22 mAh $g^{-1}$ (sample D). The difference in the initial capacity among the four samples can be attributed to the specific conductivity of the four salt electrolytes. Higher specific conductivity exhibits larger initial discharge capacity. Sample A with $LiPF_6$ salt shows the

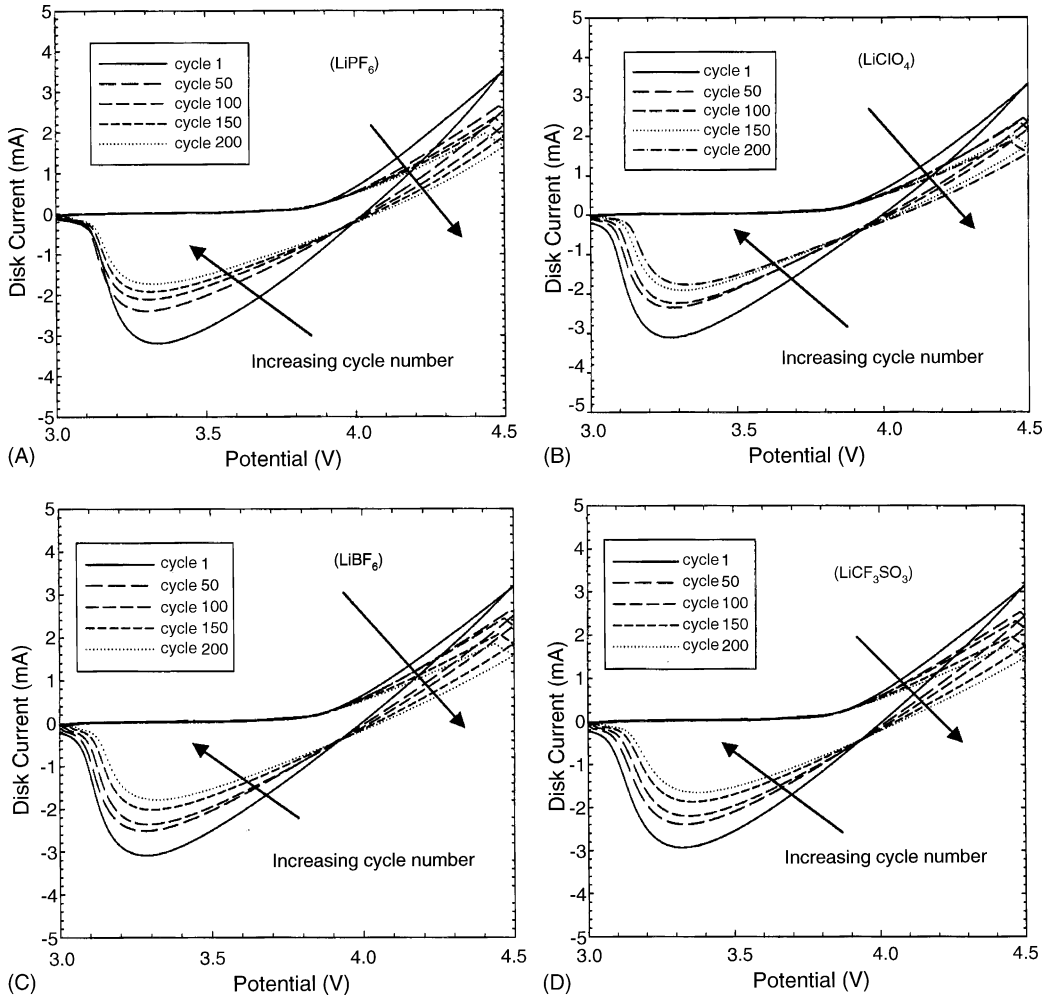


Fig. 1. Cyclic voltammogram for representative groups of spinel $LiMn_2O_4$ electrode in the beaker cell cycled between 3.0 and 4.5 V at 10 mV $s^{-1}$ and 500 rpm with various electrolyte solutions at 1, 50, 100, 150 and 200 cycles in 30 °C: (A) 1 M $LiPF_6$–EC/DMC; (B) 1 M $LiClO_4$–EC/DMC; (C) 1 M $LiBF_4$–EC/DMC; (D) 1 M $LiCF_3SO_3$–EC/DMC.

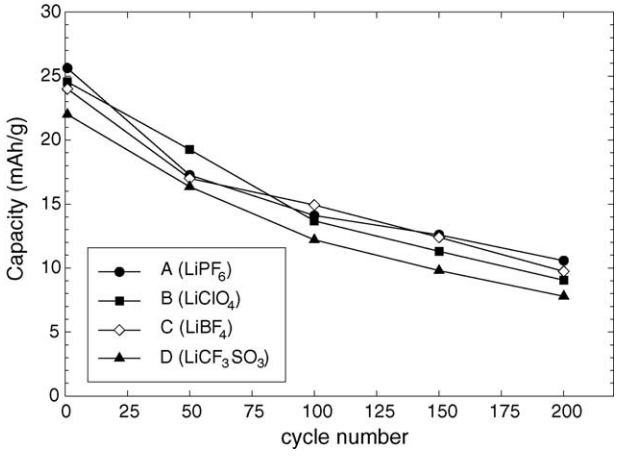


Fig. 2. Variation of the discharge capacity as a function of cycle number for representative groups of spinel $LiMn_2O_4$ electrode in the beaker cell cycled between 3.0 and 4.5 V at 10 mV $s^{-1}$ and 500 rpm with various electrolyte solutions at 1, 50, 100, 150 and 200 cycles in 30 °C: (A) 1 M $LiPF_6$–EC/DMC; (B) 1 M $LiClO_4$–EC/DMC; (C) 1 M $LiBF_4$–EC/DMC; (D) 1 M $LiCF_3SO_3$–EC/DMC at 1, 50, 100, 150 and 200 cycles in 30 °C. Capacity calculated from the cyclic voltammogram.

highest initial capacity due to the highest specific conductivity. The conductivity of $LiPF_6$ electrolyte was almost twice as high as that of $LiCF_3SO_3$ [27]. A comparison of the capacity fading in the initial 50 cycles shows that samples A and C are slightly larger than the others. The results suggest that the Mn dissolution is higher in the initial stages for $LiPF_6$ and $LiBF_4$ electrolytes. Many investigations have shown that Mn dissolution is induced by acids generated by reaction of fluorinated anions with water impurities present in the cell components (electrode, electrolytes), oxidation of the solvent, and instability of Li-based salt [4,20–25]. In the initial stage, the fresh electrolyte solutions made using anions such as $PF_6^-$ and $BF_4^-$ contain a larger amount of protons, resulting in notably high spinel dissolution. However, the influence of the solvent oxidation on the Mn dissolution becomes significant during cycling and $LiCF_3SO_3$ and $LiClO_4$ electrolytes suffer from notably high in these electrolytes, especially in the $LiCF_3SO_3$ electrolyte. It is evident that the $LiCF_3SO_3$ electrolyte is most vulnerable to solvent oxidation, whereas in the other extreme the $LiPF_6$ or $LiBF_4$ containing solvent is most inert [23]. Therefore, higher Mn dissolution in the $LiCF_3SO_3$ and $LiClO_4$ electrolytes occurs due to

Table 1
The capacity loss rate values for representative groups of spinel $LiMn_2O_4$ electrode in the beaker cell cycled between 3.0 and 4.5 V at 10 mV $s^{-1}$ and 500 rpm with various electrolyte solutions at 30 °C

| Sample group | Cycle number | Initial capacity (mAh $g^{-1}$) | Capacity loss/cycle (%) | Capacity loss after 200 cycles (%) |
|---|---|---|---|---|
| A (1 M $LiPF_6$–EC/DMC) | 200 | 25.6041 | 0.4412 | 58.7 |
| B (1 M $LiClO_4$–EC/DMC) | 200 | 24.5475 | 0.4980 | 63.2 |
| C (1 M $LiBF_4$–EC/DMC) | 200 | 24.0010 | 0.450 | 59.4 |
| D (1 M $LiCF_3SO_3$–EC/DMC) | 200 | 21.9985 | 0.5171 | 64.5 |

the large extent of solvent oxidation during the cycling. Calculations of the rate of capacity loss and the capacity per cycle are listed in Table 1; both are based on the electrode performance on the continuous cycles at a high scan rate shown in Fig. 1. The capacity loss rate, expressed as percentage per cycle, is based on the initial discharge capacity [28]. The capacities of all the samples are calculated from the CVs and exhibit an initial value of about 25.6–22 mAh $g^{-1}$ in the first discharge. Only a fraction of the actual capacity is accessible at this high sweep rate. Samples A and C with $LiPF_6$ and $LiBF_4$ electrolytes, respectively, exhibited a capacity loss of 0.45% per cycle over 200 cycles, and these were slightly lower than the 0.5% per cycle in samples B and D. In addition, compared with about 59% loss in capacity for samples A and C, both samples B and D suffer about 64% capacity loss after 200 cycles. It has been demonstrated that samples A and C exhibit a better cycling performance than samples B and D. A similar cycling performance tendency has been reported in many other papers [18,19,23].

The in situ monitoring of Mn dissolution from the spinel $LiMn_2O_4$ electrodes of samples A–D was carried out during cycling voltammetry or galvanostatic charge and discharge by means of RRDE collection experiments. Fig. 3 showed both the

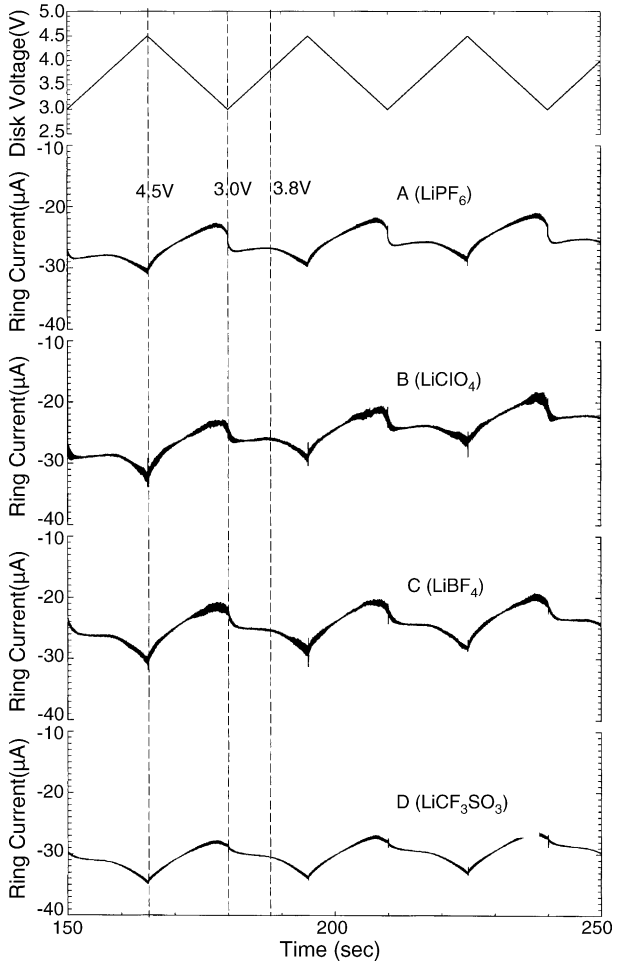


Fig. 3. RRDE profiles for $Mn^{2+}$ collection experiments conducted at room temperature and 1000 rpm at spinel disk electrode cycled between 3.0 and 4.5 V at 100 mV $s^{-1}$ and a ring electrode held at 1.0 V with different salt electrolytes at 5, 6 and 7 cycles.

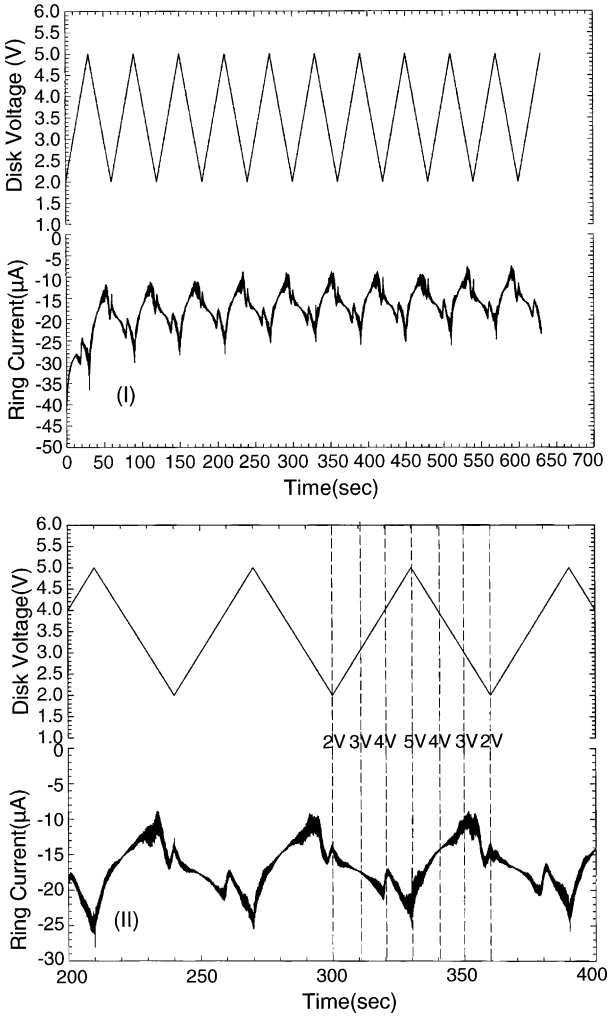


Fig. 4. RRDE profiles for $Mn^{2+}$ collection experiments conducted at room temperature and 1000 rpm at spinel ($LiMn_2O_4$) disk electrode cycled between 2.0 and 5.0 V at 100 mV $s^{-1}$ and ring electrode held at 1.0 V in 1 M $LiPF_6$ + EC/DMC (1:1) electrolyte: (I) cycles 1–10 and (II) cycles 5–7.

disk voltage and ring current profiles at the 5, 6, and 7 cycles of samples A, B, C and D between 3.0 and 4.5 V with a sweep rate of 100 mV $s^{-1}$ at room temperature. The ring electrode was held at 1.0 V with a rotation speed of 1000 rpm. In conjunction with the disk electrode, a regular shape of the ring current was observed at different cycles for all samples. The cathodic peak current at the ring indicated that some Mn atoms dissolved from the disk electrode into the electrolyte solution, forming soluble oxidized $Mn^{2+}$ ion species that were reduced on the ring electrode. Similar shaped ring cathodic currents were obtained for all samples, which exhibit the same Mn dissolution behavior as the typical spinel cell. These results indicate that Mn dissolves from the spinel $LiMn_2O_4$ electrodes in all salt electrolytes. The ring cathodic current of all samples increases from about 3.8 V (disk potential) and reaches a maximum when the disk potential is taken to 4.5 V during the charged process, as shown in Fig. 3. On the cathodic sweep, the ring cathodic current becomes noticeable at a potential below 3.2 V (disk potential) and reached a maximum when the disk potential dropped to 3.0 V. The ring currents exhibit maxima corresponding to the end-of-charge (EOC) and end-of-discharge (EOD), with the largest peak at EOC. These results indicate that dissolution of Mn from all the spinel electrodes is highest at voltage end points, with most of the Mn dissolution occurring at EOC. This is in good agreement with most of the evidences reported thus far that points to solubility at the top of charge as the major reason for the capacity fading in Li/$LiMn_2O_4$-based cells.

Although similar maximum ring currents appear in the same region of the disk potential for all the samples of different salt electrolytes, there is a noticeable difference in the values of the ring cathodic currents. The ring cathodic currents in samples A and C are smaller than those in samples B and D due to the lower dissolution of Mn rate for the spinel electrode in the $LiPF_6$ and $LiBF_4$ electrolytes. Moreover, the ring cathodic currents in samples C are smaller than those in samples A, indicating a less severe Mn dissolution for $LiBF_4$ that is more stable than $LiPF_6$ [29]. In addition, sample A ($LiPF_6$) exhibits a larger ring cathodic current at end-of-discharge, which can be attributed to

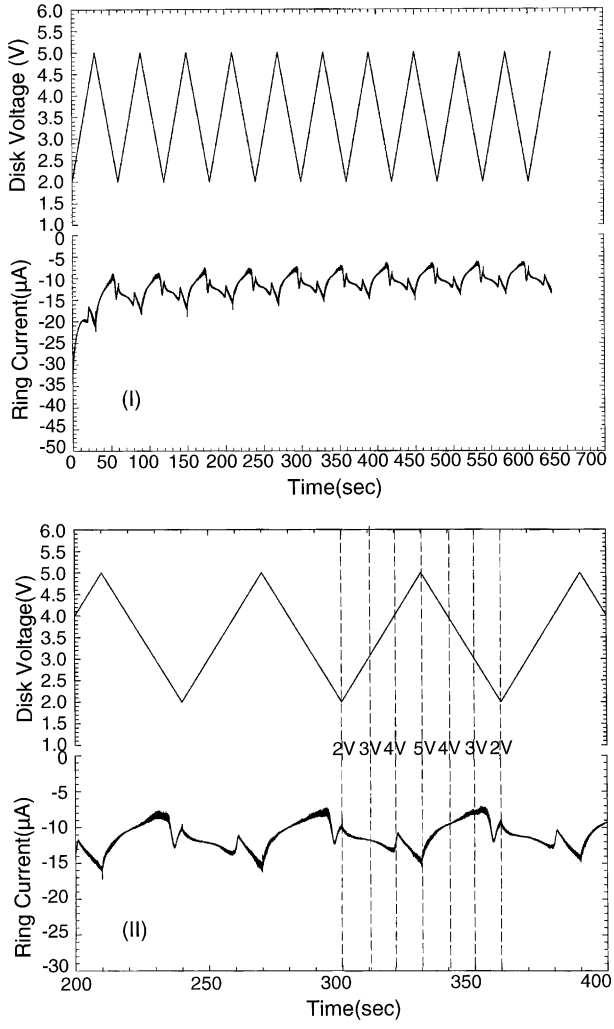


Fig. 5. RRDE profiles for $Mn^{2+}$ collection experiments conducted at room temperature and 1000 rpm at spinel ($LiMn_2O_4$) disk electrode cycled between 2.0 and 5.0 V at 100 mV $s^{-1}$ and ring electrode held at 1.0 V in 1 M $LiClO_4$ + EC/DMC (1:1) electrolyte: (I) cycles 1–10 and (II) cycles 5–7.

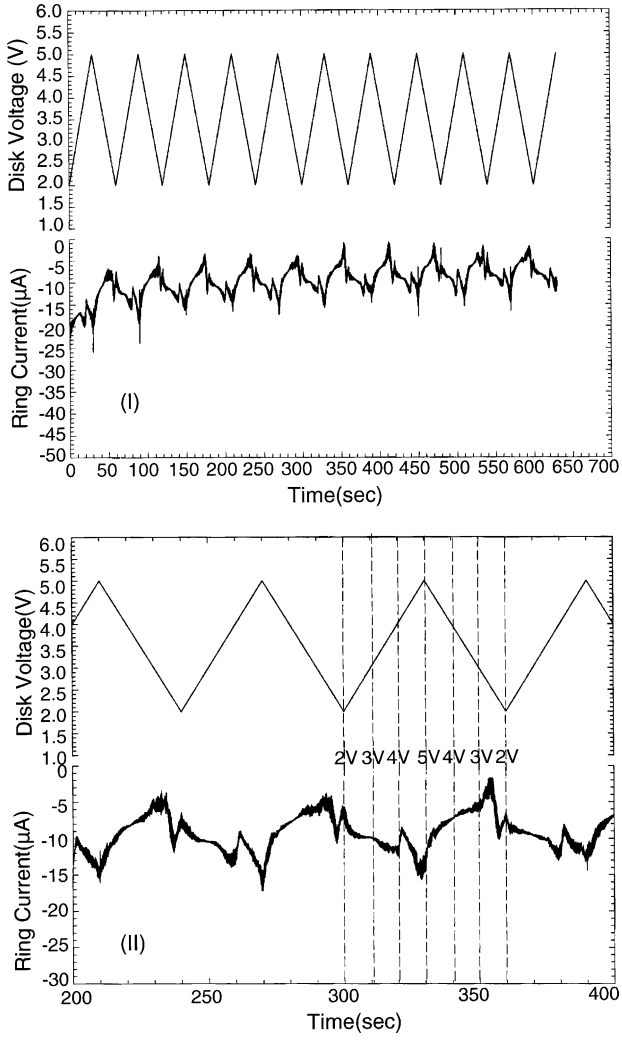


Fig. 6. RRDE profiles for $Mn^{2+}$ collection experiments conducted at room temperature and 1000 rpm at spinel ($LiMn_2O_4$) disk electrode cycled between 2.0 and 5.0 V at 100 mV $s^{-1}$ and ring electrode held at 1.0 V in 1 M $LiBF_4$ + EC/DMC (1:1) electrolyte: (I) cycles 1–10 and (II) cycles 5–7.

the higher Mn dissolution in the discharged state due to the larger amount of HF generation from the $LiPF_6$ salt decomposition [29].

In order to study the in situ monitoring of Mn dissolution during overcharge and overdischarge, the RRDE profile was examined between 2.0 and 5.0 V. Figs. 4(I), 5(I), 6(I) and 7(I) show both the disk voltage and ring current profiles for the first 10 cycles of samples A, B, C and D, respectively, between 2.0 and 5.0 V with a sweep rate of 100 mV $s^{-1}$ and room temperature. Although the wide voltage window was swept, similar results were obtained with those in the normal voltage sweep. In conjunction with the disk electrode, a regular shape of the ring current was observed after the first cycle for all samples, as shown in Figs. 4(I), 5(I), 6(I) and 7(I), respectively. The corresponding expanded RRDE profiles for cycles 5, 6 and 7 are given in Figs. 4(II), 5(II), 6(II) and 7(II). It is obvious that seven ring current maxima are observed for all samples in this voltage range. Those exhibiting Mn dissolution behavior are similar for all samples during the cycling process. The first three peaks occur at disk potentials of 2.3, 3.9 and 5.0 V on the anodic sweep while the other four peaks occur 4.5, 3.5, 2.9 and 2.3 V on the cathodic sweep. These observations suggest that the dissolution of Mn from spinel electrodes in all Li-salt electrolytes takes place during the charging process, followed by the discharging process. From the experimental results, the Mn dissolution in all the samples of different salt electrolytes occurs at the end of the charging and discharging step. In particular, Mn dissolution is accelerated at the top of the charging stage and causes capacity fading. A similar dissolution tendency has been reported in many studies [4,7–11]. However, the ring cathodic current exhibited in the $LiCF_3SO_3$–salt electrolyte (sample D) is much larger than that of the other samples, and increases sharply with cycle number, as shown in Fig. 7(I). Moreover, the peak of ring current on sample D at disk potential 5.0 V is much larger than that in other samples, as shown in Fig. 7(II). These results can be explained by the voltage breakdown of the $LiCF_3SO_3$–salt electrolyte. Within the same solvent ((DMC + EC) (1:1)), the voltage breakdown of all $LiPF_6$, $LiClO_4$ and $LiBF_4$ electrolytes is larger than 5.1 V and only that of $LiCF_3SO_3$ electrolyte is below 5 V [21]. Therefore, electrolyte oxidation occurs in the $LiCF_3SO_3$ electrolyte at high voltage (5 V), leading to the unusual behavior on the ring currents under the overcharge and overdischarge conditions.

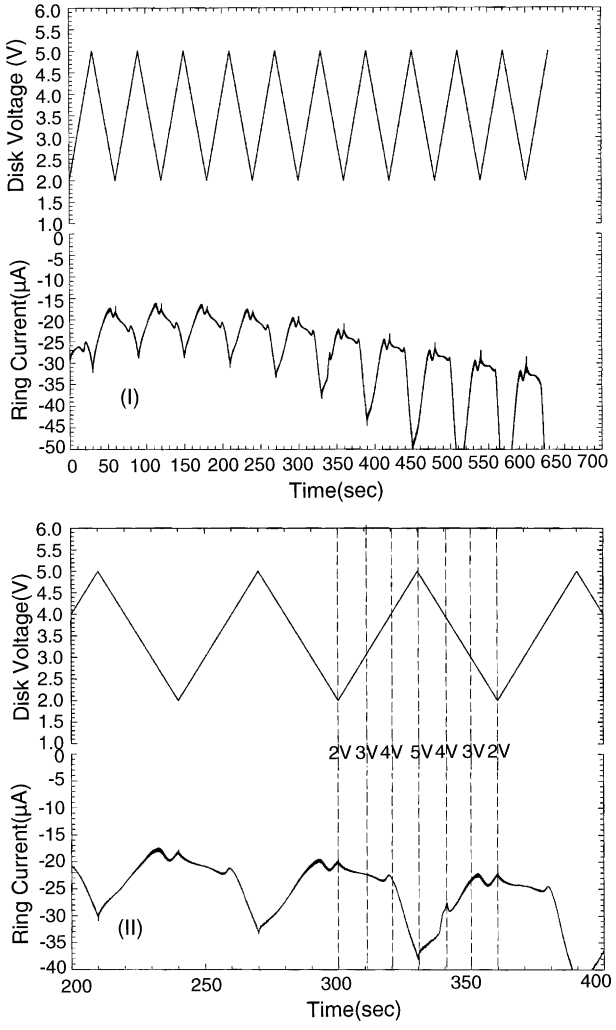


Fig. 7. RRDE profiles for $Mn^{2+}$ collection experiments conducted at room temperature and 1000 rpm at spinel ($LiMn_2O_4$) disk electrode cycled between 2.0 and 5.0 V at 100 mV $s^{-1}$ and ring electrode held at 1.0 V in 1 M $LiCF_3SO_3$ + EC/DMC (1:1) electrolyte: (I) cycles 1–10 and (II) cycles 5–7.

## 4. Conclusion

The dissolution of Mn from a thin porous spinel electrode in different Li-salted electrolytes was studied by rotating ring–disk collection experiments. Four types of electrolytes, including $LiPF_6$, $LiClO_4$, $LiBF_4$ and $LiCF_3SO_3$, in ethylene carbonate–dimethyl carbonate (EC–DMC) have been investigated to measure Mn dissolution and capacity losses in lithium-ion cells. $LiPF_6$ electrolyte shows the best cycling performance owing to the higher oxidation potential and specific conductivity. Both $LiPF_6$ and $LiBF_4$ electrolytes exhibited a capacity loss of 0.45% per cycle over 200 cycles, and these were slightly lower than 0.5% per cycle in $LiClO_4$ and $LiCF_3SO_3$ electrolytes. In addition, compared with about 59% loss in capacity for $LiPF_6$ and $LiBF_4$ electrolytes, both $LiClO_4$ and $LiCF_3SO_3$ electrolytes suffer about 64% capacity loss after 200 cycles.

The in situ monitoring of Mn dissolution from the all different electrolytes was carried out under various conditions. Similar shaped ring cathodic currents are obtained for all electrolytes, which exhibited the same Mn dissolution behavior for electrolytes. The ring currents reach maxima at the EOC and EOD, with the largest peak at the former. The results suggest that the dissolution of Mn from all electrolytes occurs during charge/discharge cycling, especially in the charged state (at >4.0 V) and discharged state (at <3.1 V). The largest peak of EOC demonstrated that Mn dissolution takes place mainly at the top of the charge. Moreover, $LiPF_6$ electrolyte exhibits a slightly larger ring cathodic current at EOD, which can be attributed to the higher Mn dissolution in the discharged state because of the larger amount of HF generation from the $LiPF_6$ salt decomposition. Under the overcharge and overdischarge conditions, higher ring cathodic currents are observed in the $LiCF_3SO_3$ electrolyte at disk potential 5.0 V and increase with cycle numbers,

which can be attributed to the lower voltage breakdown of the $LiCF_3SO_3$ electrolyte, thus leading to electrolyte oxidation.

## Acknowledgments

The authors are grateful to the National Science Council of the ROC for financial support to conduct this work under Contract No. NSC-92-2214-E-390-001. Thanks are also due to Forex Pro Enterprise Co. (Taiwan) for providing useful materials.

## References

[1] Y. Nishi, J. Power Sources 100 (2001) 101–106.
[2] G. Pistoia, A. Antonini, R. Rosati, D. Zane, Electrochim. Acta 41 (1996) 2683.
[3] A. Antonini, C. Bellitto, M. Pasquali, G. Pistoia, J. Electrochem. Soc. 145 (1998) 2726.
[4] D.H. Jang, Y.J. Shin, S.M. Oh, J. Electrochem. Soc. 143 (1996) 2204.
[5] R.J. Gummow, A. de Kock, M.M. Tackeray, Solid State Ionics 69 (1994) 59.
[6] E. Wang, D. Ofer, W. Bowden, N. Iltchev, R. Moses, K. Brandt, J. Electrochem. Soc. 147 (2000) 4023.
[7] T. Aoshima, K. Okahara, C. Kiyohara, K. Shizuka, J. Power Sources 97–98 (2001) 377.
[8] Y. Xia, Y. Zhou, M. Yoshio, J. Electrochem. Soc. 144 (1997) 2593.
[9] A. Yamada, K. Miura, K. Hinokuma, M. Tanaka, J. Electrochem. Soc. 142 (1995) 2149.
[10] M.M. Thackeray, J. Electrochem. Soc. 142 (1995) 2558.
[11] G. Pistoia, G. Wang, Solid State Ionics 66 (1993) 135.
[12] S.G. Youn, I.H. Lee, C.S. Yoon, C.K. Kim, Y.-K. Sun, Y.-S. Lee, M. Yoshio, J. Power Sources 108 (2002) 97–105.
[13] J.M. Tarascon, F. Coowar, G. Amatucci, F.K. Shokoohi, D. Guyomard, J. Electrochem. Soc. 141 (1994) 1421.
[14] Y.J. Shin, A. Manthiram, Electrochem. Solid State Lett. 5 (2002) A55–A58.
[15] H. Huang, C.A. Vincent, P.G. Bruce, J. Electrochem. Soc. 146 (1999) 3649–3654.
[16] L.-F. Wang, C.-C. Ou, K.A. Striebel, J.-S. Chen, J. Electrochem. Soc. 150 (7) (2003) A905–A911.
[17] L.-F. Wang, B.-J. Fang, J.-S. Chen, J. Power Sources 150 (2005) 1–10.
[18] K. Hayashi, Y. Nemoto, S. Tobishima, J. Yamaki, Electrochim. Acta 44 (1999) 2337.
[19] G. Moumouzias, G. Ritzoulis, D. Siapkas, D. Terzidis, J. Power Sources 122 (2003) 57–66.
[20] A.D. Pasquier, A. Blyr, P. Courjal, D. Larcher, G. Amatucci, B. Gerand, J.M. Tarascon, J. Electrochem. Soc. 146 (1999) 428.
[21] D. Guyomard, J.M. Tarascon, J. Power Sources 54 (1995) 92–98.
[22] J.H. Lee, J.K. Hong, D.H. Jang, Y.K. Sun, S.M. Oh, J. Power Sources 89 (2000) 7.
[23] D.H. Jang, Y.J. Shin, S.M. Oh, J. Electrochem. Soc. 144 (1997) 3342.
[24] D. Aubarch, Y. Gofer, J. Electrochem. Soc. 138 (1991) 3529.
[25] D. Aubarch, A. Zaban, A. Schlecter, Y. Ein-Eli, E. Zinigrad, B. Markowsky, J. Electrochem. Soc. 142 (1995) 2873.
[26] K. Dokko, S. Horikoshi, T. Itoh, M. Nishizawa, M. Mohamedi, I. Uchida, J. Power Sources 90 (2000) 109.
[27] M. Lshikawa, M. Morita, M. Asao, Y. Matsuda, J. Electrochem. Soc. 141 (1994) 1105.
[28] J.-S. Chen, L.-F. Wang, J. Power Sources 70 (1998) 269–275.
[29] A. du Pasquier, A. Blyr, A. Cressent, C. Lenain, G. Amatucci, J.M. Tarascon, J. Power Sources 81–82 (1999) 54–59.